

Article

Synthesis, Structures and Chemical Reactivity of Dithiolato-Bridged Ni-Fe Complexes as Biomimetics for the Active Site of [NiFe]-Hydrogenases

Li-Cheng Song , Shuai Chen, Xiao-Feng Han, Zhen-Qing Zhang, Yin-Peng Wang and Yi-Xiong Dong

Department of Chemistry, State Key Laboratory of Elemento-Organic Chemistry, College of Chemistry, Nankai University, Tianjin 300071, China; cs@mail.nankai.edu.cn (S.C.); 1120140199@mail.nankai.edu.cn (X.-F.H.); zzzq94666@163.com (Z.-Q.Z.); 1120200332@mail.nankai.edu.cn (Y.-P.W.); 18635638981@163.com (Y.-X.D.)

* Correspondence: lcsong@nankai.edu.cn

Abstract: To develop the structural and functional modeling chemistry of [NiFe]-H₂ases, we have carried out a study regarding the synthesis, structural characterization and reactivity of a new series of [NiFe]-H₂ase model complexes. Thus, treatment of diphosphine dppb-chelated Ni complex (dppb)NiCl₂ (dppb = 1,2-(Ph₂P)₂C₆H₄) with (dppv)Fe(CO)₂(pdt) (dppv = 1,2-(Ph₂P)₂C₂H₂, pdt = 1,3-propanedithiolate) and NaBF₄ gave dicarbonyl complex [(dppb)Ni(pdt)Fe(CO)₂(dppv)](BF₄)₂ (**[A]**(BF₄)₂). Further treatment of **[A]**(BF₄)₂ with Me₃NO and Bu₄NCN or KSCN afforded t-cyanido and t-isothiocyanato complexes [(dppb)Ni(pdt)Fe(CO)(t-R)(dppv)]BF₄ (**[1]**BF₄, R = CN; **[2]**BF₄, R = NCS), respectively. While azadiphosphine MeN(CH₂PPh₂)₂-chelated t-hydride complex [MeN(CH₂PPH₂)₂Ni(pdt)Fe(CO)(t-H)(dppv)]BF₄ (**[3]**BF₄) was prepared by treatment of dicarbonyl complex [MeN(CH₂PPH₂)₂Ni(pdt)Fe(CO)₂(dppv)](BF₄)₂ (**[B]**(BF₄)₂) with Me₃NO and 1.5 MPa of H₂, treatment of dicarbonyl complex **[B]**(BF₄)₂ with Me₃NO (without H₂) in pyridine resulted in formation of a novel monocarbonyl complex [MeN(CH₂PPH₂)₂Ni(SCHCH₂CH₂S)Fe(CO)(dppv)]BF₄ (**[4]**BF₄) via the unexpected sp³ C-H bond activation reaction. Furthermore, azadiphosphine PhN(CH₂PPh₂)₂-chelated μ-mercapto complex [PhN(CH₂PPh₂)₂Ni(pdt)Fe(CO)(μ-SH)(dppv)]BF₄ (**[5]**BF₄) was prepared by treatment of dicarbonyl complex [PhN(CH₂PPh₂)₂Ni(pdt)Fe(CO)₂(dppv)](BF₄)₂ (**[C]**(BF₄)₂) with Me₃NO and H₂S gas, whereas treatment of azadiphosphine Ph₂CHN(CH₂PPh₂)₂-chelated dicarbonyl complex [Ph₂CHN(CH₂PPh₂)₂Ni(pdt)Fe(CO)₂(dppe)](BF₄)₂ (**[D]**(BF₄)₂, dppe = 1,2-(Ph₂P)₂C₂H₄) with Me₃NO·2H₂O gave rise to μ-hydroxo complex [Ph₂CHN(CH₂PPh₂)₂Ni(pdt)Fe(CO)(μ-OH)(dppe)]BF₄ (**[6]**BF₄). All the possible pathways for formation of the new model complexes are briefly discussed, and their structures were fully characterized by various spectroscopic techniques and for six of them by X-ray crystallography.

Keywords: [NiFe]-hydrogenase; biomimetic models; dinuclear NiFe complexes; bioinorganic; X-ray crystallography



Citation: Song, L.-C.; Chen, S.; Han, X.-F.; Zhang, Z.-Q.; Wang, Y.-P.; Dong, Y.-X. Synthesis, Structures and Chemical Reactivity of Dithiolato-Bridged Ni-Fe Complexes as Biomimetics for the Active Site of [NiFe]-Hydrogenases. *Inorganics* **2022**, *10*, 90. <https://doi.org/10.3390/inorganics1007090>

Academic Editors: Wolfgang Linert, Duncan H. Gregory, Richard Dronskowski, Vladimir Arion, Claudio Pettinari and Torben R. Jensen

Received: 22 May 2022

Accepted: 21 June 2022

Published: 24 June 2022

Publisher's Note: MDPI stays neutral with regard to jurisdictional claims in published maps and institutional affiliations.



Copyright: © 2022 by the authors. Licensee MDPI, Basel, Switzerland. This article is an open access article distributed under the terms and conditions of the Creative Commons Attribution (CC BY) license (<https://creativecommons.org/licenses/by/4.0/>).

1. Introduction

Hydrogenases (H₂ases) are a class of biological enzymes that catalyze the reversible interconversion of H₂ ⇌ 2H⁺ + 2e⁻ in various microorganisms such as bacteria, archaea, and some eukaryotes [1–3]. According to the metal composition in their active site, H₂ases are generally divided into three main groups [NiFe]-H₂ases [4–6], [FeFe]-H₂ases [7–9] and [Fe]-H₂ase [10–12]. Among the three enzymes, [NiFe]-H₂ases are the oldest and most widely distributed in nature [13,14].

X-ray crystallographic study revealed that the active site of [NiFe]-H₂ases consists of two metal centers in which the Ni center is coordinated by two terminal cysteinate ligands, the Fe center is coordinated by one terminal CO/two terminal CN⁻ ligands, and the two metal centers are combined together by two bridging cysteinate ligands [15–18]. To date, the H₂ activation function catalyzed by the [NiFe]-H₂ase active site is known to involve several

states, such as the Ni-SIa, Ni-R and Ni-C states [19–21]. While Ni-SIa, and Ni-R states all contain a diamagnetic butterfly $\text{Ni}^{\text{II}}\text{Fe}^{\text{II}}(\mu\text{-S})_2$ core, the Ni-C state contains a paramagnetic $\text{Ni}^{\text{III}}\text{Fe}^{\text{II}}(\mu\text{-S})_2$ core. In addition, the Ni-R, and Ni-C states involve an additional $\mu\text{-H}$ ligand, while the Ni-SIa state does not have any other bridging ligand except the two $\mu\text{-S}$ ligands in its $\text{Ni}^{\text{II}}\text{Fe}^{\text{II}}(\mu\text{-S})_2$ core (Figure 1).

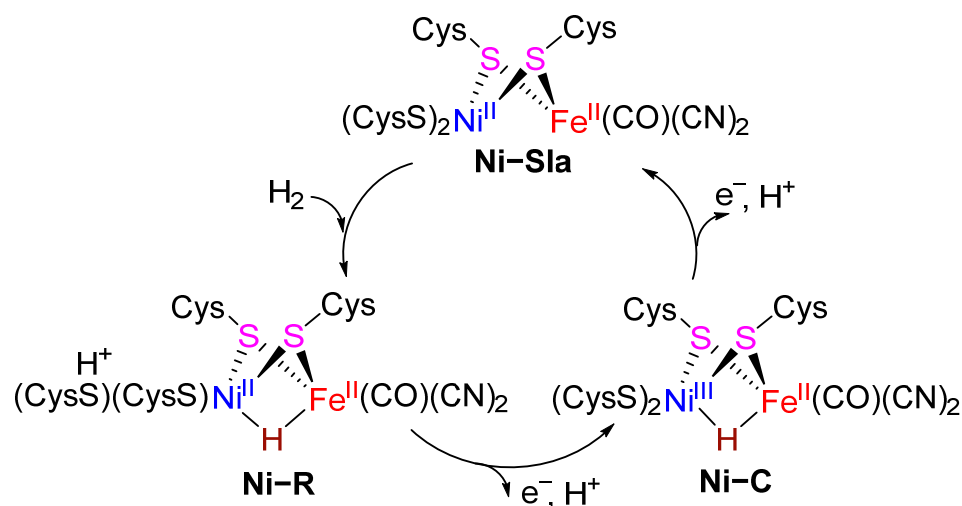


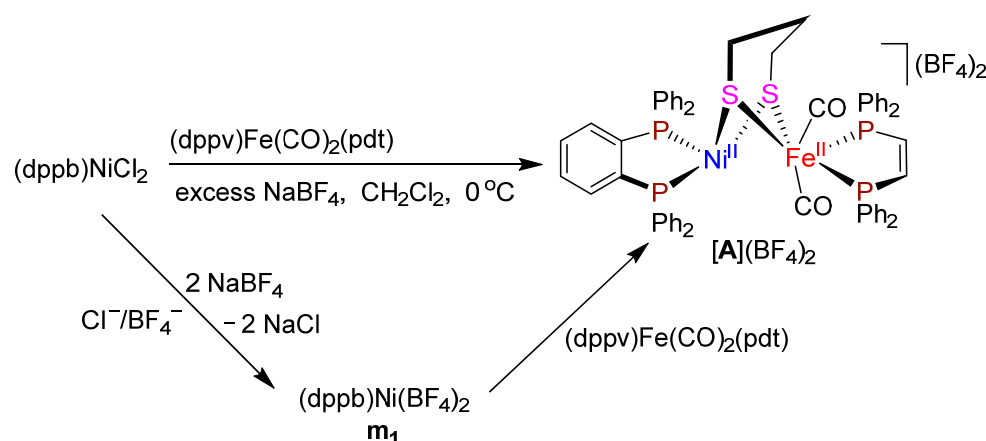
Figure 1. Some states of [NiFe]-H₂ases associated with a suggested catalytic cycle for H₂ activation.

The well-elucidated active site structure and the identified states of the active site during H₂ activation catalyzed by [NiFe]-H₂ases have promoted researchers to synthesize a wide variety of [NiFe]-H₂ase models [22–45]. In recent years, we have prepared some [NiFe]-H₂ase model complexes and some of them were proved to be functional models of [NiFe]-H₂ases [35,37,38,42–45]. To develop the biomimetic chemistry of [NiFe]-H₂ases and to understand the reversible H₂ activation catalyzed by [NiFe]-H₂ases, we further designed and synthesized a series of new dithiolato-bridged [NiFe]-H₂ase biomimetics. In this article, we report their synthetic procedures, structural characterization and chemical reactivity.

2. Results and Discussion

2.1. Synthesis and Characterization of Diphosphine dppb-Chelated Dicarbonyl Complex $[(\text{dppb})\text{Ni}(\text{pdt})\text{Fe}(\text{CO})_2(\text{dppv})](\text{BF}_4)_2$ (**[A]**)(BF_4)₂ and Monocarbonyl Complexes $[(\text{dppb})\text{Ni}(\text{pdt})\text{Fe}(\text{CO})(\text{t-R})(\text{dppv})]\text{BF}_4$ (**[1]**)(BF_4 , R = CN; **[2]**)(BF_4 , R = NCS)

We found that diphosphine dppb (dppb = 1,2-(Ph₂P)₂C₆H₄)-chelated dicarbonyl complex **[A]**(BF_4)₂ could be prepared by treatment of a CH₂Cl₂ solution of mononuclear Ni complex (dppb)NiCl₂ with one equimolar Fe complex (dppv)Fe(CO)₂(pdt) (dppv = 1,2-(PPh₂)₂C₂H₂, pdt = 1,3-propanedithiolate) and a large excess of NaBF₄ in 80% yield (Scheme 1). The formation of dicarbonyl complex **[A]**(BF_4)₂ might be suggested to involve two elementary reaction steps: (i) the doubly anionic Cl[−]/BF₄[−] exchange between (dppb)NiCl₂ and NaBF₄ to give intermediate **m**₁; and (ii) coordination of the two S atoms in pdt ligand of (dppv)Fe(CO)₂(pdt) to Ni atom of the resulting intermediate **m**₁ to afford the final product [45] (Scheme 1).



Scheme 1. Synthesis of dicarbonyl complex $[A](BF_4)_2$.

Dicarbonyl complex $[A](BF_4)_2$ is an air-stable orange-red solid. The IR spectrum of $[A](BF_4)_2$ shows one very strong absorption band at 1997 cm^{-1} for its terminal carbonyls. The $^{31}\text{P}\{^1\text{H}\}$ NMR spectrum displays one singlet at 56.9 ppm for its two P atoms in the Ni-bound dppb ligand and one singlet at 65.1 ppm for its two P atoms in the Fe-bound dppv ligand, respectively. In addition, the ^1H NMR and $^{13}\text{C}\{^1\text{H}\}$ NMR spectra are in good agreement with its structure shown in Scheme 1.

The molecular structure of $[A](BF_4)_2$ was determined by X-ray crystallography. As shown in Figure 2, this complex comprises one dication $[(dppb)Ni(pdt)Fe(CO)_2(dppv)]^{2+}$ and two BF_4^- monoanions. In its dication, a dithiolato pdt ligand is bridged between the NiFe centers to form a butterfly $Ni^{II}Fe^{II}(\mu-S)_2$ core with a “hinge” angle 45.88° between the two Ni1S1Fe1 and Ni1S2Fe1 planes. While the Ni center adopts a distorted square-planar geometry, the Fe center adopts a pseudo-octahedral geometry. The $Ni\cdots Fe$ distance (3.1875 \AA) in $[A](BF_4)_2$ is much longer than that (2.57 \AA) in D. Volgaris Miyazaki F. $[NiFe]-H_2ase$ [19] and much longer than the sum (2.56 \AA) of Ni and Fe atom covalent radii [46]. This implies that there isn't any metal-metal bonding interaction between its NiFe centers.

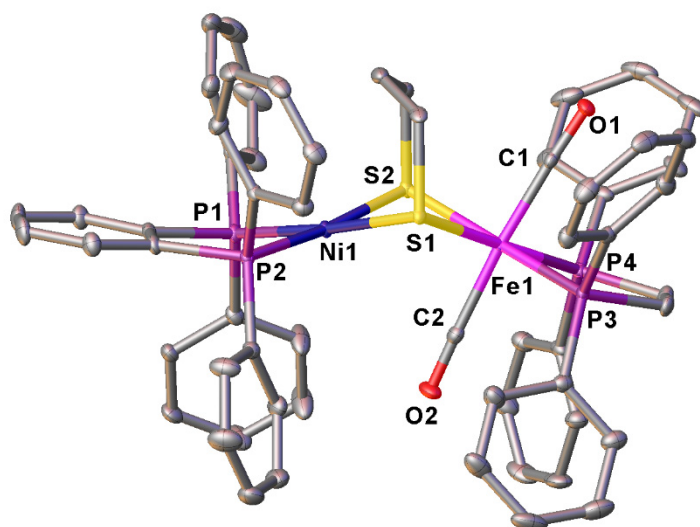
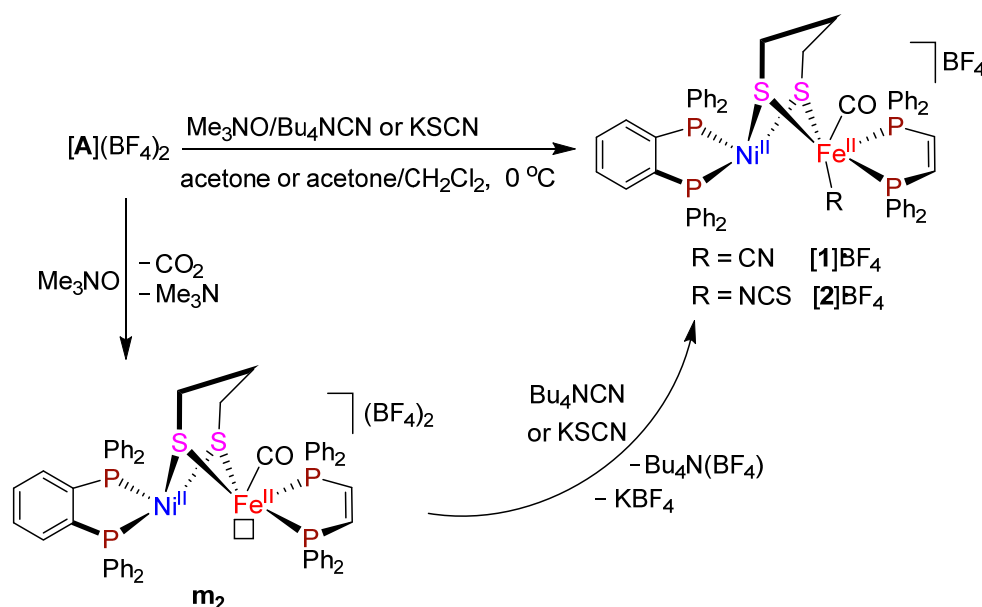


Figure 2. Molecular structure of $[A](BF_4)_2$ with thermal ellipsoids drawn at a 30% probability level. All H atoms and two BF_4^- anions are omitted for the sake of clarity. Selected bond lengths (\AA) and angles ($^\circ$): $Ni\cdots Fe$ 3.1875, $Ni1-S1$ 2.2301(11), $Ni1-S2$ 2.2314(12), $Fe1-S1$ 2.3106(11), $Fe1-S2$ 2.3235(11), $Fe1-P3$ 2.2330(12), $Fe1-P4$ 2.2426(12), $Ni1-P1$ 2.1585(12), $Ni1-P2$ 2.1647(12); $S1-Ni1-S2$ $84.03(4)$, $P1-Ni1-S1$ $175.93(5)$, $P1-Ni1-P2$ $87.54(4)$, $S1-Fe1-S2$ $80.24(4)$, $P3-Fe1-S1$ $92.74(4)$, $P3-Fe1-P4$ $87.34(4)$.

After dicarbonyl complex $[A](BF_4)_2$ was prepared, we further prepared the diphosphine dppb-chelated monocarbonyl complexes $[1]BF_4$ and $[2]BF_4$. Thus, when complex $[A](BF_4)_2$ was treated with one equiv of decarbonylation agent Me_3NO in acetone followed by treatment of the resulting mixture with one equiv of Bu_4NCN or $KSCN$, the corresponding t-cyanido and t-isothiocyanato complexes $[1]BF_4$ and $[2]BF_4$ were produced in 68% and 63% yields, respectively (Scheme 2).



Scheme 2. Synthesis of t-cyanido complex $[1]BF_4$ and t-isothiocyanato complex $[2]BF_4$.

A possible pathway suggested for the formation of complexes $[1]BF_4$ and $[2]BF_4$ is shown in Scheme 2, which involves the following two reaction steps. The first step involves decarbonylation of dicarbonyl complex $[A](BF_4)_2$ under the action of decarbonylating agent Me_3NO to give 5-coordinate intermediate m_2 with a vacant site trans to its pdt ligand [47]. The second step involves the nucleophilic attack of the negatively-charged C atom in CN group of Bu_4NCN or the nucleophilic attack of the paired electrons on N atom in NCS group of $KSCN$ (note that the SCN group in $KSCN$ is a well-known ambidentate ligand) [48] at the positively-charged Fe atom followed by loss of one molecule of $Bu_4N(BF_4)$ or KBF_4 to produce the final t-cyanido and t-isothiocyanato complexes.

Both $[1]BF_4$ and $[2]BF_4$ are air-stable orange-red solids. The IR spectra of the two complexes show one very strong absorption band at 1956 and 1950 cm^{-1} for their terminal carbonyls and one additional absorption band at 2067 cm^{-1} for the $N=C=S$ ligand in $[2]BF_4$. In addition, the $^{13}C\{^1H\}$ NMR spectra of $[1]BF_4$ and $[2]BF_4$ exhibit one singlet at 214.4 and 215.5 ppm for their terminal carbonyl C atoms, respectively. The $^{31}P\{^1H\}$ NMR spectra of the two complexes, similar to dicarbonyl complex $[A](BF_4)_2$, display one singlet at $51.9/55.3\text{ ppm}$ for their two P atoms in the Ni-bound dppb ligands and one singlet at $76.6/73.6\text{ ppm}$ for their two P atoms in the Fe-bound dppv ligands, respectively. The assignment of the lower field singlets to the two P atoms in the dppv ligands is based on the fact that the $^{31}P\{^1H\}$ NMR signal of $(dppv)(CO)_2Fe(pdt)$ determined under the same conditions was found in the lower field at 79.3 ppm .

The molecular structures of $[1]BF_4$ and $[2]BF_4$ were confirmed by X-ray crystal diffraction analysis. As shown in Figures 3 and 4, the two complexes are isostructural. Both of them consist of one monocation $[(dppb)Ni(pdt)Fe(CO)(CN)(dppv)]^+$ or $[(dppb)Ni(pdt)Fe(CO)(NCS)(dppv)]^+$ and one BF_4^- monoanion. The NiFe centers of $[1]BF_4$ and $[2]BF_4$ are bridged by a dithiolato pdt ligand to form a butterfly $Ni^{II}Fe^{II}(\mu-S)_2$ core and the “hinge” angles between their $Ni1S1Fe1$ and $Ni1S2Fe1$ planes are 45.97 and 47.16° , respectively. The $C2\equiv N1$ bond length in $[1]BF_4$ is 1.144 \AA , whereas the $N1=C2$ and $C2=S3$ bond lengths in $[2]BF_4$ are 1.145 \AA and 1.626 \AA , respectively. The $Ni\cdots Fe$ distances of $[1]BF_4$ (3.2106 \AA)

and $[2]BF_4$ (3.1570 Å) are very close to that of $[A](BF_4)_2$. Therefore, like $[A](BF_4)_2$, they do not have any Ni \cdots Fe metal-metal bonding interaction. Notably, complex $[2]BF_4$ is the first prepared and crystallographically characterized N=C=S ligand-containing [NiFe]-H₂ase model, although some CN ligand-containing [NiFe]-H₂ase models were previously reported by other groups [24,49].

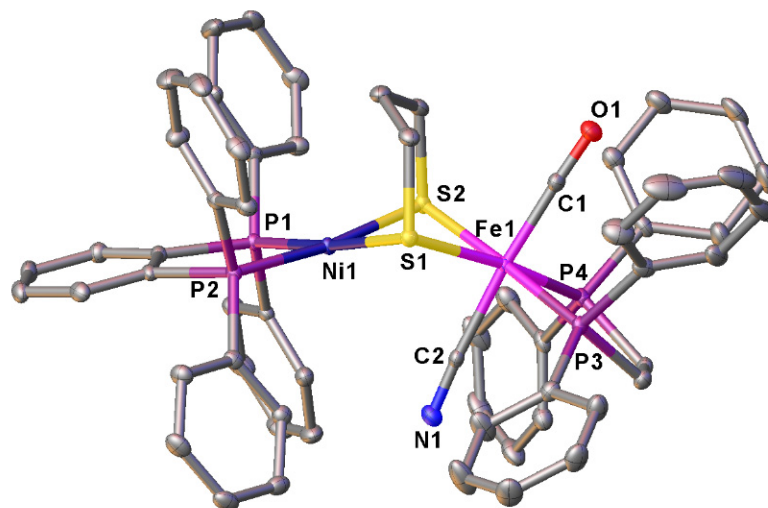


Figure 3. Molecular structure of $[1]BF_4$ with thermal ellipsoids drawn at a 30% probability level. All H atoms and one BF_4^- anion are omitted for the sake of clarity. Selected bond lengths (Å) and angles ($^\circ$): Ni \cdots Fe 3.2106, Ni1-S1 2.2500(8), Ni1-S2 2.2258(8), Fe1-S1 2.3360(8), Fe1-S2 2.3186(8), Fe1-P3 2.2226(8), Fe1-P4 2.2203(8), Ni1-P1 2.1667(8), C2-N1 1.144(4); S1-Ni1-S2 83.72(3), P1-Ni1-S1 173.76(3), P1-Ni1-P2 88.50(3), S1-Fe1-S2 79.84(3), P3-Fe1-S1 99.10(3), P3-Fe1-P4 86.13(3).

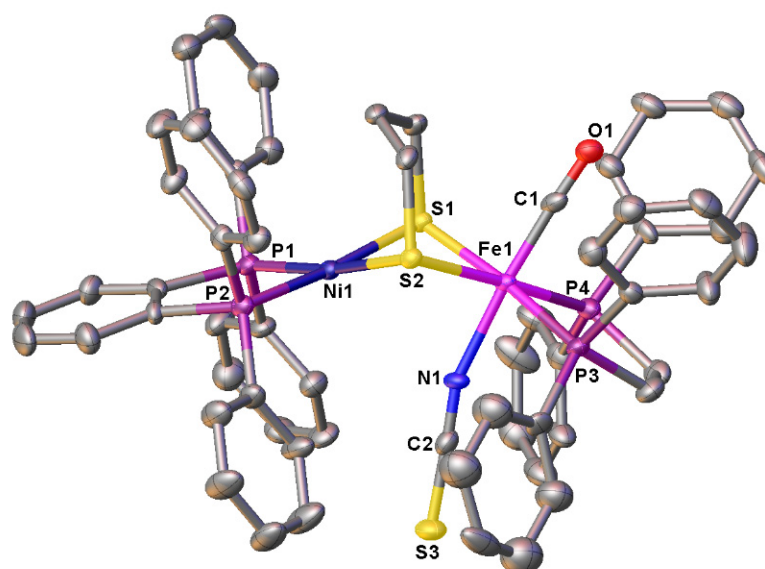
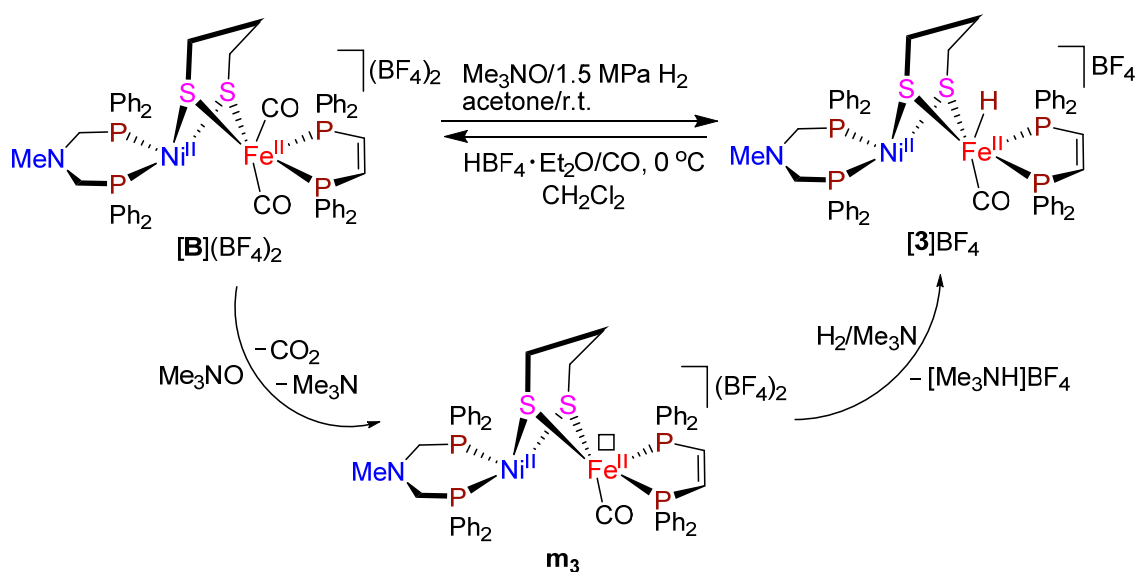


Figure 4. Molecular structure of $[2]BF_4$ with thermal ellipsoids drawn at a 30% probability level. All H atoms and one BF_4^- anion are omitted for the sake of clarity. Selected bond lengths (Å) and angles ($^\circ$): Ni \cdots Fe 3.1570, Ni1-S1 2.2343(19), Ni1-S2 2.235(2), Fe1-S1 2.3390(19), Fe1-S2 2.3199(18), Fe1-P3 2.232(2), Ni1-P1 2.169(2), C2-N1 1.145(9), C2-S3 1.626(7); S1-Ni1-S2 85.00(7), P1-Ni1-S1 93.09(8), P1-Ni1-P2 89.30(8), S1-Fe1-S2 80.79(6), P3-Fe1-S1 174.89(8), P3-Fe1-P4 86.85(7).

2.2. Reactions of $\text{MeN}(\text{CH}_2\text{PPh}_2)_2$ -Chelated Dicarbonyl Complex

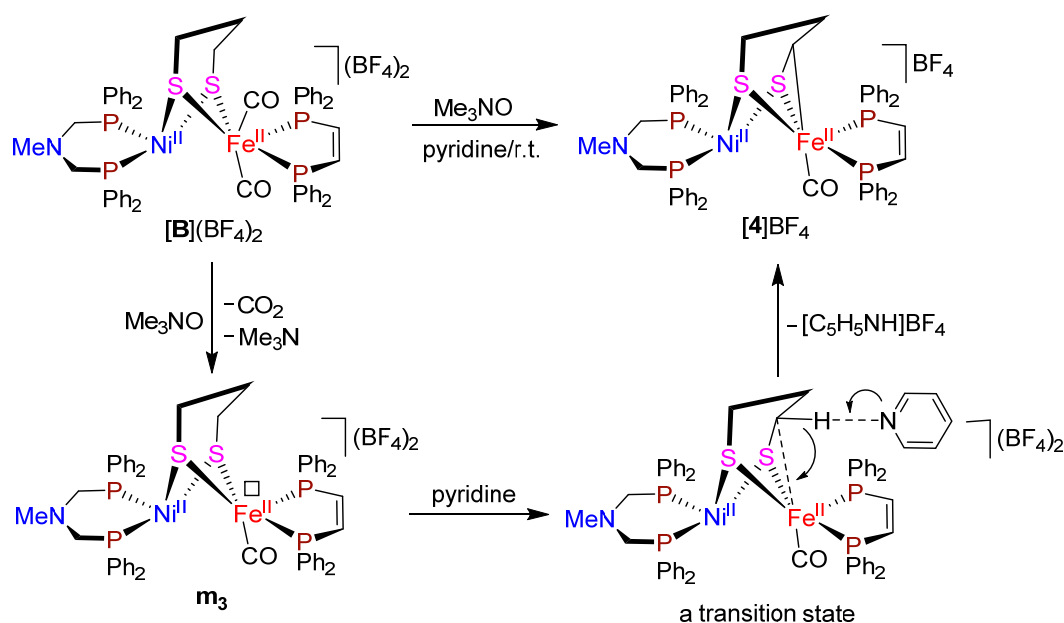
$[\text{MeN}(\text{CH}_2\text{PPh}_2)_2\text{Ni}(\text{pdt})\text{Fe}(\text{CO})_2(\text{dppv})](\text{BF}_4)_2$ (**[B]** $(\text{BF}_4)_2$) Leading to Monocarbonyl Complexes
 $[\text{MeN}(\text{CH}_2\text{PPh}_2)_2\text{Ni}(\text{pdt})\text{Fe}(\text{CO})(\text{t-H})(\text{dppv})]\text{BF}_4$ (**[3]** BF_4) and
 $[\text{MeN}(\text{CH}_2\text{PPh}_2)_2\text{Ni}(\text{SCHCH}_2\text{CH}_2\text{S})\text{Fe}(\text{CO})(\text{dppv})]\text{BF}_4$ (**[4]** BF_4)

In 2017, we reported the preparation of an azadiphosphine $\text{PhN}(\text{CH}_2\text{PPh}_2)_2$ -chelated t-hydride $[\text{NiFe}]\text{-H}_2$ ase model [42]. In order to see if the azadiphosphine $\text{MeN}(\text{CH}_2\text{PPh}_2)_2$ -chelated dicarbonyl complex **[B]** $(\text{BF}_4)_2$ [45] (an analogue of the diphosphine *dppb*-chelated dicarbonyl complex **[A]** $(\text{BF}_4)_2$) could also activate H_2 to give the corresponding $\text{MeN}(\text{CH}_2\text{PPh}_2)_2$ -chelated t-hydride complex **[3]** BF_4 , we carried out the reaction of **[B]** $(\text{BF}_4)_2$ with one equiv of decarbonylating agent Me_3NO and 1.5 MPa of H_2 ; as a result, the expected t-hydride complex **[3]** BF_4 was produced in 78% yield, indicating that complex **[B]** $(\text{BF}_4)_2$ possesses the H_2 activation function (Scheme 3). Similar to the previously reported $\text{PhN}(\text{CH}_2\text{PPh}_2)_2$ -chelated t-hydride complex [42], the formation of the $\text{MeN}(\text{CH}_2\text{PPh}_2)_2$ -chelated t-hydride complex **[3]** BF_4 might be suggested to involve two reaction steps. The first step involves the formation of decarbonylating intermediate **m**₃ with a vacant site cis to its *pdt* ligand for H_2 coordination. The second step involves heterolytic cleavage of the coordinated H_2 under the assistance of in situ generated proton acceptor Me_3N to give the final t-hydride product (Scheme 3). In addition, it should be noted that when t-hydride complex **[3]** BF_4 was treated with excess $\text{HBF}_4 \cdot \text{Et}_2\text{O}$ and with bubbling CO gas, it could be converted to dicarbonyl complex **[B]** $(\text{BF}_4)_2$ in 81% yield (Scheme 3).



Scheme 3. Synthesis of t-hydride complex **[3]** BF_4 .

More interestingly, except H_2 activation, dicarbonyl complex **[B]** $(\text{BF}_4)_2$ was further found to have the sp^3 C-H bond activation function [50]. Thus, when dicarbonyl complex **[B]** $(\text{BF}_4)_2$ was treated in pyridine with an equimolar Me_3NO (without H_2), a novel sp^3 C-Fe bond-containing monocarbonyl complex **[4]** BF_4 was produced via the intramolecular sp^3 C-H bond activation of **[B]** $(\text{BF}_4)_2$ in 73% yield (Scheme 4). It is interesting to note that complex **[B]** $(\text{BF}_4)_2$ is the first $[\text{NiFe}]\text{-H}_2$ ase model to have the C-H bond activation function.



Scheme 4. Synthesis of the sp^3 C-Fe bond-containing monocarbonyl complex [4]BF₄.

As shown in Scheme 4, the formation of complex [4]BF₄ might be suggested to include three reaction steps. The first step involves the formation of 5-coordinate intermediate **m**₃ as indicated in Scheme 3. The second step includes a transition state formed by interaction of one sp^3 C-H bond directly attached to S atom of the pdt ligand in intermediate **m**₃ with pyridine N atom and the positively-charged Fe atom. The final step affords product [4]BF₄ accompanied by formation of the pyridinium salt [C₅H₅NH]BF₄.

While t-hydride complex [3]BF₄ is an air-stable deep-green solid, the sp^3 C-Fe bond-containing complex [4]BF₄ is an air-stable grey-black solid. The IR spectra of the two complexes show one very strong absorption band at 1912 and 1911 cm^{-1} for their terminal carbonyls, respectively. The ³¹P{¹H} NMR spectrum of [3]BF₄ exhibits one singlet at 7.2 ppm for its two P atoms in the Ni-bound azadiphosphine ligand and another singlet at 91.4 ppm for its two P atoms in the Fe-bound dppv ligand. In addition, [4]BF₄ displays two doublets at 3.9/11.4 ppm for its two P atoms in the Ni-bound azadiphosphine ligand and two doublets at 93.2/94.7 ppm for its two P atoms in the Fe-bound dppv ligands since it is an asymmetric molecule. The ¹H NMR spectrum of [3]BF₄ displays one singlet at 2.54 ppm for its CH₃N group and one triplet at −4.19 ppm with $J = 74$ Hz for its terminal hydride, which is very close to that (−4.27 ppm, $J = 74$ Hz) displayed by its azadiphosphine PhN(CH₂PPh₂)₂-chelated analogue [42].

Fortunately, the molecular structure of [4]BF₄ was successfully determined by X-ray crystallography (Figure 5). This molecule is composed of one monocation [MeN(CH₂PPh₂)₂-Ni(SCHCH₂CH₂S)Fe(CO)(dppv)]⁺ and one BF₄[−] monoanion. In its monocation there is one sp^3 C-Fe bond, namely the C27-Fe1 bond formed by interaction of one sp^3 C-H bond attached directly to S atom of the bridging pdt ligand with pyridine N atom and the positively-charged Fe atom. The C27-Fe1 bond length is 2.067 Å, whereas the Ni⋯Fe distance is 2.9751 Å. While the Ni atom adopts a distorted square-planar geometry, the Fe atom has a pseudo-octahedral geometry. The “hinge” angle between its two Ni1S1Fe1 and Ni2S2Fe1 planes is 49.14°, which is obviously larger than that (45.97°) in monocarbonyl complex [1]BF₄ or that (47.16°) in complex [2]BF₄, presumably owing to formation of the intramolecular C27-Fe1 bond in monocarbonyl complex [4]BF₄.

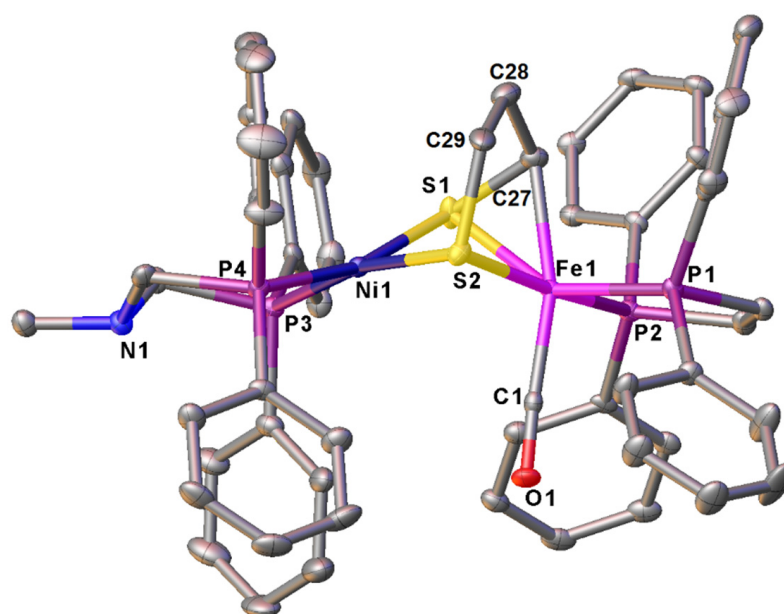
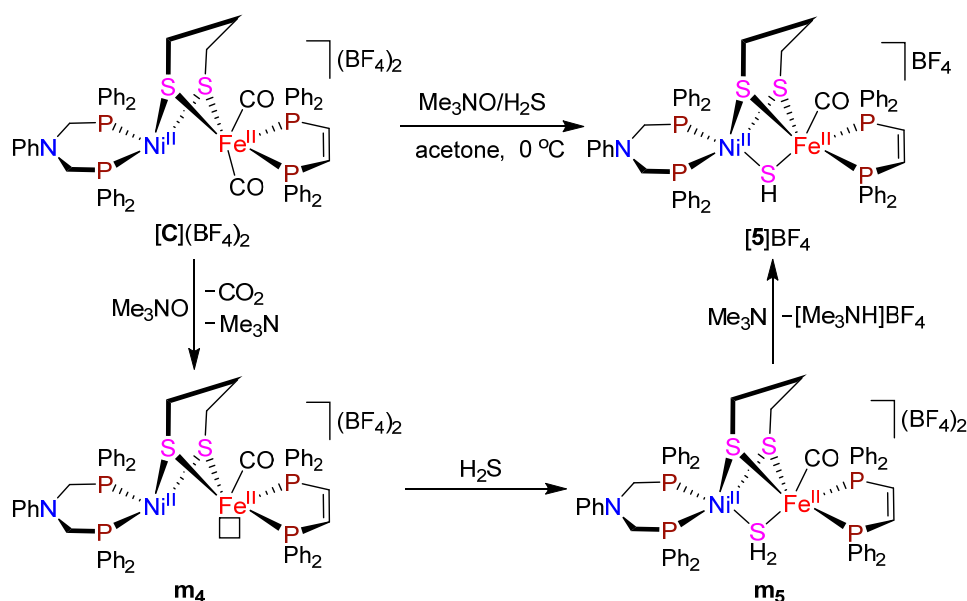


Figure 5. Molecular structure of $[4]BF_4$ with thermal ellipsoids drawn at a 30% probability level. All H atoms and one BF_4^- anion are omitted for the sake of clarity. Selected bond lengths (Å) and angles ($^\circ$): Ni \cdots Fe 2.9751, Ni1-S1 2.1805(14), Ni1-S2 2.2103(14), Fe1-S1 2.3330(14), Fe1-S2 2.2755(14), Fe1-P1 2.1735(14), Fe1-P2 2.1969(13), Ni1-P3 2.2005(14), Ni1-P4 2.1718(14); S1-Ni1-S2 88.67(5), P3-Ni1-S1 89.95(5), P3-Ni1-P4 93.19(5), S1-Fe1-S2 83.48(5), P1-Fe1-S1 148.21(6), P1-Fe1-P2 86.71(5).

2.3. Reaction of Azadiphosphine $PhN(CH_2PPh_2)_2$ -Chelated Dicarbonyl Complex $[PhN(CH_2PPh_2)_2Ni(pdt)Fe(CO)_2(dppv)](BF_4)_2$ ($[C](BF_4)_2$) Leading to Monocarbonyl Complex $[PhN(CH_2PPh_2)_2Ni(pdt)Fe(CO)(\mu-SH)(dppv)]BF_4$ ($[5]BF_4$)

The azadiphosphine $PhN(CH_2PPh_2)_2$ -chelated μ -mercapto complex $[5]BF_4$ was found to be prepared by reaction of the corresponding dicarbonyl complex $[PhN(CH_2PPh_2)_2Ni(pdt)Fe(CO)_2(dppv)](BF_4)_2$ ($[C](BF_4)_2$) [42], an analogue of the diphosphine dppb-chelated dicarbonyl complex $[A](BF_4)_2$, with one equiv of decarbonylating agent Me_3NO in acetone followed by treatment of the resulting mixture with bubbling H_2S gas in nearly quantitative yield (Scheme 5).



Scheme 5. Synthesis of μ -mercapto complex $[5]BF_4$.

A possible pathway for the formation of μ -mercapto complex $[5]BF_4$ is shown in Scheme 5. The first step in Scheme 5 is similar to that shown in Scheme 2 to involve the formation of 5-coordinate intermediate m_4 . The second step involves coordination of one molecule of H_2S to the positively-charged Fe center of m_4 to afford intermediate m_5 . The final step involves deprotonation from μ -SH₂ ligand with the aid of in situ generated proton acceptor Me_3N to produce $[5]BF_4$.

μ -Mercapto complex $[5]BF_4$ is an air-stable brown solid. The IR spectrum of $[5]BF_4$ displays one very strong absorption band at 1938 cm^{-1} for its terminal carbonyl. The 1H NMR spectrum exhibits one triplet at -2.89 ppm for its μ -SH ligand. The $^{31}P\{^1H\}$ NMR spectrum exhibits two singlets at -1.3 and 73.6 ppm for two P atoms in its azadiphosphine and dppv ligands, respectively.

The X-ray crystallographic study indicated that complex $[5]BF_4$ contains one monocation $[PhN(CH_2PPh_2)_2Ni(pdt)Fe(CO)(\mu\text{-SH})(dppv)]^+$ and one monoanion BF_4^- (Figure 6). While the Ni center adopts a distorted square-pyramidal geometry, the Fe center adopts a pseudo-octahedral geometry. The most striking feature of $[5]BF_4$ is to contain a bridging μ -SH ligand, which is unsymmetrically bridged between its NiFe centers with the Ni1–S3 and Fe1–S3 distances being 2.5968 and 2.3444 Å, respectively. It should be noted that complex $[5]BF_4$ is the first prepared and crystallographically characterized μ -SH ligand-containing $[NiFe]$ -H₂ase model.

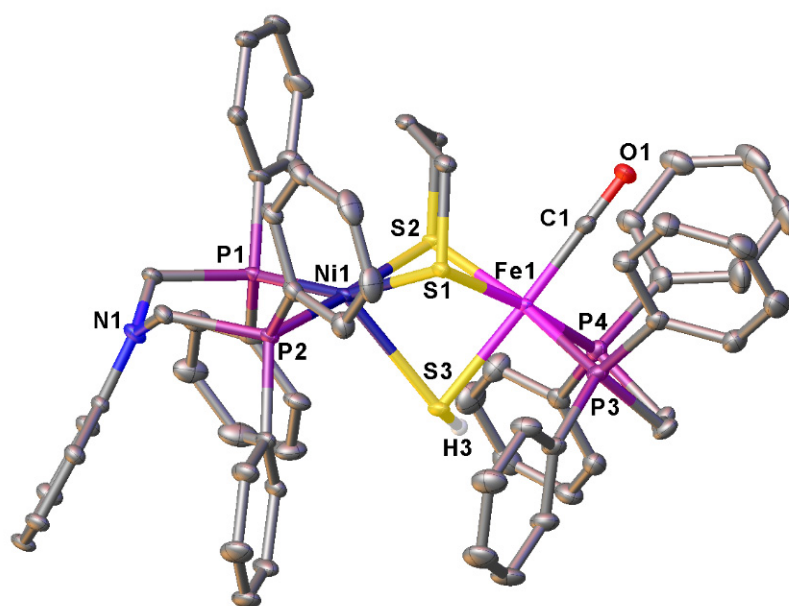
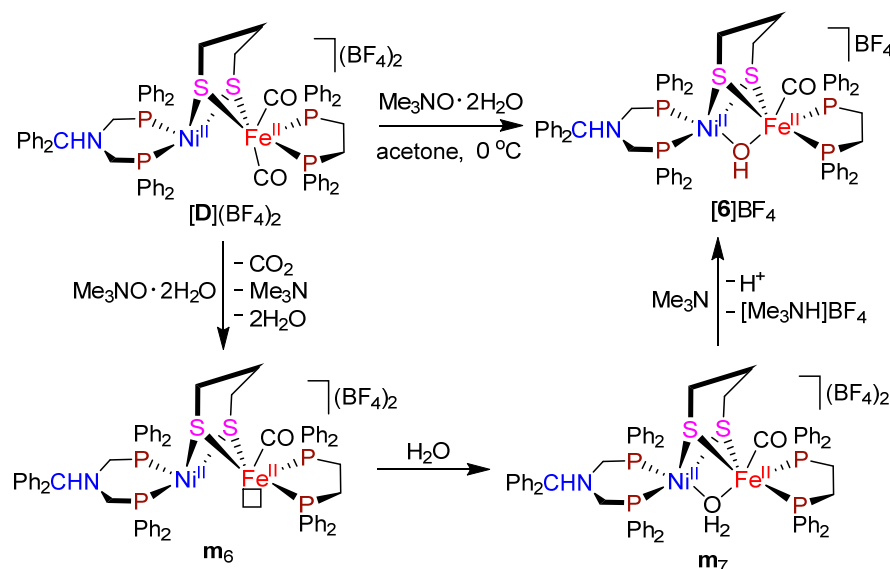


Figure 6. Molecular structure of $[5](BF_4)$ with thermal ellipsoids drawn at a 30% probability level. All H atoms except that on the μ -SH ligand and one BF_4^- anion are omitted for the sake of clarity. Selected bond lengths (Å) and angles ($^\circ$): Ni \cdots Fe 3.1002, Ni1–S1 2.2668(10), Ni1–S3 2.5968(9), Fe1–S1 2.2798(9), Fe1–S3 2.3444(9), Fe1–P3 2.2168(10), Fe1–P4 2.2201(10), Ni1–P1 2.1919(10), Ni1–P2 2.2093(9); S1–Ni1–S2 81.12(3), P1–Ni1–S1 159.20(4), P1–Ni1–P2 95.80(4), S1–Fe1–S2 79.76(3), P3–Fe1–S1 93.34(4), P3–Fe1–P4 86.95(4).

2.4. Synthesis and Characterization of Azadiphosphine $Ph_2CHN(CH_2PPh_2)_2$ -Chelated Dicarbonyl Complex $[Ph_2CHN(CH_2PPh_2)_2Ni(pdt)Fe(CO)_2(dppe)](BF_4)_2$ ($[D](BF_4)_2$) and Monocarbonyl Complex $[Ph_2CHN(CH_2PPh_2)_2Ni(pdt)Fe(CO)(\mu\text{-OH})(dppe)]BF_4$ ($[6]BF_4$)

Similar to the preparation of diphosphine dppb-chelated complex $[A](BF_4)_2$, the azadiphosphine $Ph_2CHN(CH_2PPh_2)_2$ -chelated complex $[D](BF_4)_2$ was found to be prepared by treatment of a CH_2Cl_2 solution of mononuclear Ni complex $[Ph_2CHN(CH_2PPh_2)_2]NiCl_2$ with 1 equiv of mononuclear Fe complex $(dppe)Fe(CO)_2(pdt)$ ($dppe = 1,2\text{-}(Ph_2P)_2C_2H_4$) and a large excess of $NaBF_4$ in 80% yield. Furthermore, we found that when complex $[D](BF_4)_2$ was treated with 1 equiv of the hydrated trimethylamine oxide, an azadiphosphine $Ph_2CHN(CH_2PPh_2)_2$ -chelated μ -hydroxo complex $[6]BF_4$ was isolated in 65% yield

(Scheme 6). Similar to the previously reported azadiphosphine $\text{PhN}(\text{CH}_2\text{PPh}_2)_2$ -chelated μ -hydroxo analogue [42], the formation of μ -hydroxo complex $[\mathbf{6}]\text{BF}_4$ could be suggested to include the following three reaction steps. The first step involves decarbonylation of dicarbonyl complex $[\mathbf{D}](\text{BF}_4)_2$ to give intermediate \mathbf{m}_6 with a vacant coordination site trans to its pdt ligand [47]. The second step involves coordination of \mathbf{m}_6 with one molecule of in situ liberated H_2O from $\text{Me}_3\text{NO}\cdot 2\text{H}_2\text{O}$ to afford μ -aqua intermediate \mathbf{m}_7 . The third step involves deprotonation of the μ -aqua intermediate \mathbf{m}_7 with the aid of Me_3N to afford μ -hydroxo complex $[\mathbf{6}]\text{BF}_4$ (Scheme 6).



Scheme 6. Synthesis of dicarbonyl complex $[\mathbf{D}](\text{BF}_4)_2$ and μ -hydroxo complex $[\mathbf{6}]\text{BF}_4$.

While dicarbonyl complex $[\mathbf{D}](\text{BF}_4)_2$ is an air-stable orange-red solid, μ -hydroxo complex $[\mathbf{6}]\text{BF}_4$ is an air-stable orange-red solid. The IR spectra of $[\mathbf{D}](\text{BF}_4)_2$ and $[\mathbf{6}]\text{BF}_4$ display one very strong absorption band at 1983 and 1917 cm^{-1} for their terminal carbonyls, respectively. The $^{31}\text{P}\{^1\text{H}\}$ NMR spectra of $[\mathbf{D}](\text{BF}_4)_2$ and $[\mathbf{6}]\text{BF}_4$ exhibit one singlet at 4.9 and 2.2 ppm for their two P atoms attached to the Ni-bound azadiphosphine ligand and one singlet at 56.8 and 65.8 ppm for their two P atoms attached to the Fe-bound dppe ligand, respectively. The ^1H NMR spectra of $[\mathbf{D}](\text{BF}_4)_2$ and $[\mathbf{6}]\text{BF}_4$ display one singlet at 4.93 and 4.51 ppm for the methyne H atom in their CHPh_2 groups, respectively. In addition, μ -hydroxo complex $[\mathbf{6}]\text{BF}_4$ exhibits another singlet at -3.39 ppm for its bridging μ -hydroxo ligand, which is slightly downfield shifted relative to the -3.66 ppm displayed by the previously reported azadiphosphine $\text{PhN}(\text{CH}_2\text{PPh}_2)_2$ -chelated μ -hydroxo analogue [42].

The molecular structure of $[\mathbf{D}](\text{BF}_4)_2$ was unequivocally confirmed by X-ray crystal diffraction analysis (Figure 7). The structure of this molecule is very similar to that of dicarbonyl complex $[\mathbf{A}](\text{BF}_4)_2$. For example, it contains one dication $\text{Ph}_2\text{CHN}(\text{CH}_2\text{PPh}_2)_2\text{Ni}(\text{pdt})\text{Fe}(\text{CO})_2(\text{dppe})]^{2+}$ and two BF_4^- monoanion. The dithiolato pdt ligand is bridged between its NiFe centers to construct a butterfly $\text{Ni}^{\text{II}}\text{Fe}^{\text{II}}(\mu\text{-S})_2$ core. While the Ni center adopts a distorted square-planar geometry, the Fe center takes a pseudo-octahedral geometry. The $\text{Ni}\cdots\text{Fe}$ distance (3.2957 \AA) in this molecule is very close to that (3.1875 \AA) of $[\mathbf{A}](\text{BF}_4)_2$.

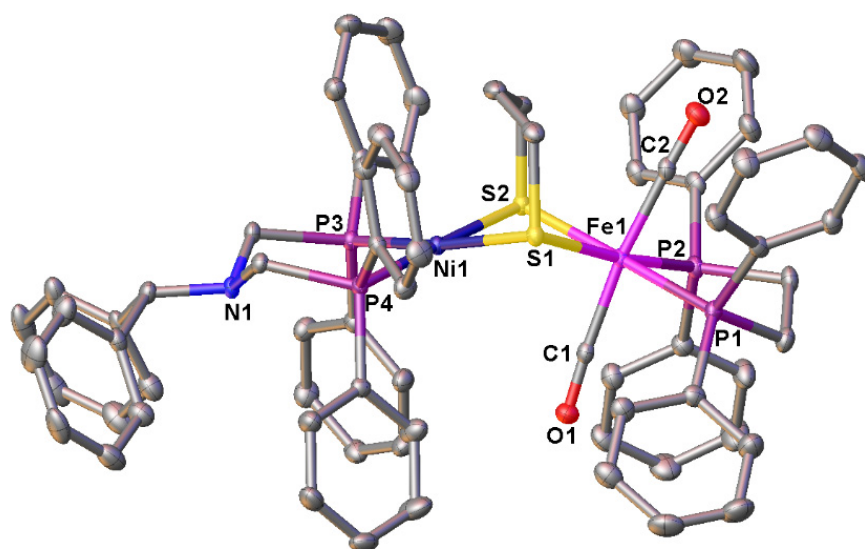


Figure 7. Molecular structure of $[D](BF_4)_2$ with thermal ellipsoids drawn at a 30% probability level. All H atoms and two BF_4^- anions are omitted for the sake of clarity. Selected bond lengths (Å) and angles ($^\circ$): Ni \cdots Fe 3.2957, Ni1-S1 2.2409(9), Ni1-S2 2.2329(9), Fe1-S1 2.3456(9), Fe1-S2 2.3013(9), Fe1-P1 2.2498(10), Fe1-P2 2.2667(10), Ni1-P3 2.1921(10), Ni1-P4 2.2063(9); S1-Ni1-S2 81.86(3), P3-Ni1-S1 170.33(4), P3-Ni1-P4 93.97(3), S1-Fe1-S2 78.21(3), P1-Fe1-S1 99.26(4), P1-Fe1-P2 87.87(4).

3. Experimental

3.1. General Comments

All reactions were performed using standard Schlenk and vacuum-line techniques under an atmosphere of highly purified N_2 or argon. While CH_2Cl_2 was distilled under argon from CaH_2 , acetone was distilled from anhydrous K_2CO_3 . Pyridine, $NaBF_4$, Me_3NO , $Me_3NO \cdot 2H_2O$, Bu_4NCN , $KSCN$, $HBF_4 \cdot Et_2O$ (50–55% in Et_2O) and other reagents were available commercially and used as received. H_2S gas was produced from reaction of $NaHS$ and H_3PO_4 . $(dppb)NiCl_2$ ($dppb = 1,2-(Ph_2P)_2C_6H_4$) [51], $(dppv)Fe(CO)_2(pdt)$ ($dppv = 1,2-(Ph_2P)_2C_2H_2$, $pdt = 1,3$ -propanedithiolate) [52], $(dppe)Fe(CO)_2(pdt)$ ($dppe = 1,2-(Ph_2P)_2C_2H_4$) [52], $[MeN(CH_2PPh_2)_2Ni(pdt)Fe(CO)_2(dppv)](BF_4)_2$ ($[B](BF_4)_2$) [45] and $[PhN(CH_2PPh_2)_2Ni(pdt)Fe(CO)_2(dppv)](BF_4)_2$ ($[C](BF_4)_2$) [42] were prepared according to the published procedures. 1H , $^{13}C\{^1H\}$ and $^{31}P\{^1H\}$ NMR spectra were obtained on a Bruker Avance 400 NMR spectrometer. IR spectra were recorded on a Bruker tensor 27 infrared spectrophotometer. Elemental analyses were performed on an Elementar Vario EL analyzer. Melting points were determined on a SGW X-4 melting point apparatus with a microscope and were uncorrected.

3.2. Synthesis of Model Complexes

$[(dppb)Ni(pdt)Fe(CO)_2(dppv)](BF_4)_2$ ($[A](BF_4)_2$): A 100 mL three-necked flask fitted with a magnetic stir-bar, two serum caps, and a nitrogen inlet tube was charged with $(dppb)NiCl_2$ (0.288 g, 0.50 mmol), $(dppv)Fe(CO)_2(pdt)$ (0.307, 0.50 mmol), $NaBF_4$ (0.550 g, 5.0 mmol) and CH_2Cl_2 (30 mL). The mixture was stirred at $0^\circ C$ for 5 h. Solvent was removed at reduced pressure and the residue was subjected to column chromatography (silica gel). Elution with CH_2Cl_2 /acetone ($v/v = 12:1$) developed a major orange-red band, from which $[A](BF_4)_2$ (0.517 g, 80%) was obtained as an orange-red solid, mp $177^\circ C$ (dec). Anal. calcd for $C_{61}H_{52}B_2F_8FeNiO_2P_4S_2$: C, 56.65; H, 4.05. Found: C, 56.39; H, 4.54. IR (KBr disk): $\nu_{C=O}$ 1997 (vs) cm^{-1} . 1H NMR (400 MHz, acetone- d_6): δ 2.16–2.20, 2.60–2.69 (2m, 6H, $CH_2CH_2CH_2$), 7.28–7.85 (m, 44H, C_6H_4 , $8C_6H_5$), 8.68–8.84 (m, 2H, $CH=CH$) ppm. $^{13}C\{^1H\}$ NMR (100 MHz, acetone- d_6): δ 33.3, 34.8, 37.8 (3s, $CH_2CH_2CH_2$), 130.7–135.8 (m, C_6H_4 , C_6H_5), 139.7–151.2 (m, $CH=CH$), 207.9, 208.3 (2s, $C\equiv O$) ppm. $^{31}P\{^1H\}$ NMR (162 MHz, acetone- d_6): δ 56.9 (s, NiP_2), 65.1 (s, FeP_2) ppm.

[(dppb)Ni(pdt)Fe(CO)(t-CN)(dppv)]BF₄ ([1]BF₄): A 50 mL three-necked flask fitted with a magnetic stir-bar, two serum caps, and a nitrogen inlet tube was charged with [A](BF₄)₂ (0.129 g, 0.10 mmol), Me₃NO (7.5 mg, 0.10 mmol) and acetone (10 mL). The mixture was stirred at 0 °C for 15 min and then a CH₂Cl₂ (5 mL) solution of Bu₄NCN (0.027 mg, 0.10 mmol) was added. After the new mixture was stirred at 0 °C for 1 h, solvent was removed at reduced pressure to leave a residue, which was subjected to silica gel column chromatography. Elution with CH₂Cl₂/acetone (*v/v* = 15:1) developed a major orange-red band, from which [1]BF₄ (0.082 g, 68%) was obtained as an orange-red solid, mp 180–182 °C. Anal. calcd for C₆₁H₅₂BF₄FeNNiOP₄S₂: C, 60.83; H, 4.35; N, 1.16. Found: C, 60.59; H, 4.54; N, 1.07. IR (KBr disk): $\nu_{C\equiv O}$ 1956 (vs) cm⁻¹. ¹H NMR (400 MHz, acetone-*d*₆): δ 2.21, 2.82 (2s, 6H, CH₂CH₂CH₂), 7.16–8.46 (m, 46H, C₆H₄, 8C₆H₅, CH=CH) ppm. ¹³C{¹H} NMR (100 MHz, acetone-*d*₆): δ 24.4, 32.3, 37.8 (3s, CH₂CH₂CH₂), 128.5–136.8 (m, C₆H₄, C₆H₅), 141.7–150.7 (m, CH=CH), 214.4 (s, C≡O) ppm. ³¹P{¹H} NMR (162 MHz, acetone-*d*₆): δ 51.9 (s, NiP₂), 76.6 (s, FeP₂) ppm.

[(dppb)Ni(pdt)Fe(CO)(t-SCN)(dppv)]BF₄ ([2]BF₄): The same procedure as that for preparation of [1]BF₄ was followed, except that Bu₄NCN was replaced by KSCN (9.7 mg, 0.10 mmol). [2]BF₄ (0.078 g, 63%) was obtained as an orange-red solid, mp 155 °C (dec). Anal. calcd for C₆₁H₅₂BF₄FeNNiOP₄S₃: C, 59.25; H, 4.24; N, 1.13. Found: C, 59.45; H, 4.17; N, 1.07. IR (KBr disk): $\nu_{N=C=S}$ 2067 (s); $\nu_{C\equiv O}$ 1950 (vs) cm⁻¹. ¹H NMR (400 MHz, CDCl₃): δ 2.06–2.65 (m, 6H, CH₂CH₂CH₂), 7.14–8.03 (m, 46H, C₆H₄, 8C₆H₅, CH=CH) ppm. ¹³C{¹H} NMR (100 MHz, CDCl₃): δ 30.2, 37.1 (2s, CH₂CH₂CH₂), 127.0–134.4 (m, C₆H₄, C₆H₅), 140.3–149.0 (m, CH=CH), 215.5 (s, C≡O) ppm. ³¹P{¹H} NMR (162 MHz, acetone-*d*₆): δ 55.3 (s, NiP₂), 73.6 (s, FeP₂) ppm.

[MeN(CH₂PPh₂)₂Ni(pdt)Fe(CO)(t-H)(dppv)]BF₄ ([3]BF₄): In an argon-filled glove box, a mixture of [MeN(CH₂PPh₂)₂Ni(pdt)Fe(CO)₂(dppv)](BF₄)₂ ([B](BF₄)₂) (0.128 g, 0.10 mmol), Me₃NO (7.5 mg, 0.10 mmol), and acetone (3 mL) was added to a 30 mL autoclave's inner sleeve (made of PTFE) containing a magnetic stir-bar. The reaction mixture was stirred at 0 °C for 10 min and then it was frozen by inserting the sleeve into liquid nitrogen. After the autoclave was sealed, the head space of the sleeve was evacuated and was refilled with 1.5 MPa of H₂. The frozen reaction mixture was thawed and then the reaction mixture was stirred at room temperature for 4 h. Solvent was removed at reduced pressure to give a residue, which was subjected to column chromatography (silica gel G). Elution with CH₂Cl₂/acetone (*v/v* = 8:1) developed a deep-green band, from which [3]BF₄ (0.090 g, 78%) was obtained as a deep-green solid, mp 119 °C (dec). Anal. calcd for C₅₇H₅₆BF₄FeNNiOP₄S₂: C, 59.00; H, 4.86; N, 1.21. Found: C, 58.84; H, 5.15; N, 1.34. IR (KBr disk): $\nu_{C\equiv O}$ 1912 (vs) cm⁻¹. ¹H NMR (400 MHz, acetone-*d*₆): δ -4.19 (t, *J* = 74 Hz, 1H, Fe-H), 1.31–1.95 (m, 6H, CH₂CH₂CH₂), 2.54 (s, 3H, CH₃N), 3.43–3.79 (m, 4H, CH₂NCH₂), 7.24–7.95 (m, 42H, 8C₆H₅, CH=CH) ppm. ¹³C{¹H} NMR (100 MHz, CDCl₃): δ 28.7, 31.9, 34.8 (3s, CH₂CH₂CH₂), 49.8 (s, CH₃N), 55.5–55.9 (m, CH₂NCH₂), 127.0–134.4 (m, C₆H₅), 148.4–149.1 (m, CH=CH), 215.4 (s, C≡O) ppm. ³¹P{¹H} NMR (162 MHz, CDCl₃): δ 7.2 (s, NiP₂), 91.4 (s, FeP₂) ppm.

[MeN(CH₂PPh₂)₂Ni(SCHCH₂CH₂S)Fe(CO)(dppv)]BF₄ ([4]BF₄): A 100 mL three-necked flask fitted with a magnetic stir-bar, two serum caps, and a nitrogen inlet tube was charged with [B](BF₄)₂ (0.127 g, 0.10 mmol), Me₃NO (7.5 mg, 0.10 mmol) and pyridine (50 mL). The mixture was stirred at room temperature for 3 h and then hexane (250 mL) was added to give a precipitate, which was subjected to column chromatography (silica gel). Elution with CH₂Cl₂/acetone (*v/v* = 20:1) developed one black band, from which [4]BF₄ (0.085 g, 73%) was obtained as a grey-black solid, mp 158–159 °C. Anal. calcd for C₅₇H₅₄BF₄FeNNiOP₄S₂: C, 59.10; H, 4.70; N, 1.21. Found: C, 58.83; H, 4.71; N, 1.13. IR (KBr disk): $\nu_{C\equiv O}$ 1911 (vs) cm⁻¹. ¹H NMR (400 MHz, CDCl₃): δ 2.31–2.77, 3.34–3.74 (2m, 12H, CHCH₂CH₂, CH₃N, CH₂NCH₂), 6.60–7.89 (m, 42H, 8C₆H₅, CH=CH) ppm. ¹³C{¹H} NMR (100 MHz, CD₂Cl₂): δ 28.9–31.1 (m, SCH₂CH₂, CH₃N), 49.6, 50.5 (2s, CH₂NCH₂), 60.7 (s, SCHFe), 122.4–138.8 (m, C₆H₅), 146.9–153.1 (m, CH=CH), 214.6 (s, C≡O) ppm. ³¹P{¹H} NMR (162 MHz, acetone-*d*₆): δ 3.9, 11.4 (2d, NiP₂), 93.2, 94.7 (2d, FeP₂) ppm.

[PhN(CH₂PPh₂)₂Ni(pdt)Fe(CO)(μ-SH)(dppv)]BF₄ ([5]BF₄): A 50 mL three-necked flask fitted with a magnetic stir-bar, two serum caps, and a nitrogen inlet tube was charged with [C](BF₄)₂ (0.134 g, 0.10 mmol), Me₃NO (7.5 mg, 0.10 mmol) and acetone (10 mL). The mixture was stirred for 15 min at 0 °C and then dry H₂S gas was bubbled into the mixture for 1 h. Solvent was removed at reduced pressure and the residue was subjected to column chromatography (silica gel). Elution with CH₂Cl₂/acetone (*v/v* = 12:1) developed a major brown band, from which [5]BF₄ (0.123 g, 98%) was obtained as a brown solid, mp 180 °C (dec). Anal. calcd for C₆₂H₅₈BF₄FeNNiOP₄S₃: C, 59.36; H, 4.66; N, 1.12. Found: C, 59.20; H, 4.90; N, 1.21. IR (KBr disk): $\nu_{C\equiv O}$ 1938 (vs) cm⁻¹. ¹H NMR (400 MHz, acetone-*d*₆): δ -2.89 (t, *J* = 8.0 Hz, 1H, SH), 1.77–2.83 (m, 6H, CH₂CH₂CH₂), 3.97–4.30 (m, 4H, CH₂NCH₂), 6.52–7.82 (m, 45H, 9C₆H₅), 8.05–8.19 (m, 2H, CH=CH) ppm. ¹³C{¹H} NMR (100 MHz, acetone-*d*₆): δ 26.2, 29.2, 33.8 (3s, CH₂CH₂CH₂), 51.9, 52.1 (2s, CH₂NCH₂), 116.9–134.2 (m, C₆H₅), 148.3–150.8 (m, CH=CH), 214.2 (s, C≡O) ppm. ³¹P{¹H} NMR (162 MHz, acetone-*d*₆): δ -1.3 (s, NiP₂), 73.6 (FeP₂) ppm.

[Ph₂CHN(CH₂PPh₂)₂Ni(pdt)Fe(CO)₂(dppe)](BF₄)₂ ([D](BF₄)₂):

(i) Ph₂CHN(CH₂PPh₂)₂: A 100 mL three-necked flask fitted with a magnetic stir-bar, two serum caps, and a reflux condenser topped with a nitrogen inlet tube was charged with polyformaldehyde (0.213 g, 7.10 mmol) and toluene (30 mL). After the mixture was stirred and slowly warmed to 70 °C, Ph₂CHNH₂ (0.646 g, 3.53 mmol) and Ph₂PH (1.35 mL, 7.75 mmol) were added. The new mixture was stirred at 70 °C for 7 h and then solvent was removed at reduced pressure to leave a residue. The residue was dissolved in EtOH (50 mL). After the solution was cooled in a refrigerator for over 1 h, the white precipitate was filtered out and washed sequentially with EtOH and Et₂O to give Ph₂CHN(CH₂PPh₂)₂ (1.636 g, 80%) as a white solid. Anal. calcd for C₃₉H₃₅NP₂: C, 80.81; H, 6.09; N, 2.42. Found: C, 80.95; H, 5.95; N, 2.19. IR (KBr disk): ν_{P-N-P} 871 (m) cm⁻¹. ¹H NMR (400 MHz, CDCl₃): δ 3.84 (s, 4H, CH₂NCH₂), 5.48 (s, CHPh₂), 7.18–7.46 (m, 30H, 6C₆H₅) ppm. ¹³C{¹H} NMR (100 MHz, CDCl₃): δ 55.2 (s, CH₂NCH₂), 72.5 (s, CHPh₂), 126.9–141.5 (m, C₆H₅) ppm. ³¹P{¹H} NMR (162 MHz, CDCl₃): δ -29.3 (s, PPh) ppm.

(ii) [Ph₂CHN(CH₂PPh₂)₂]NiCl₂: A 100 mL three-necked flask fitted with a magnetic stir-bar, two serum caps, and a nitrogen inlet tube was charged with NiCl₂·6H₂O (1.188 g, 5.00 mmol) and EtOH (20 mL). To this stirred solution was slowly added a CH₂Cl₂ (10 mL) solution of Ph₂CHN(CH₂PPh₂)₂ (2.898 g, 5.00 mmol). After the new mixture was stirred at room temperature for 6 h, solvent was removed at reduced pressure to leave a residue, which was washed sequentially with EtOH and Et₂O to give [Ph₂CHN(CH₂PPh₂)₂]NiCl₂ (2.802 g, 79%) as an orange-red solid, mp 207 °C (dec). Anal. calcd for C₃₉H₃₅Cl₂NNiP₂: C, 66.05; H, 4.97; N, 1.97. Found: C, 66.10; H, 4.75; N, 1.71. IR (KBr disk): ν_{P-N-P} 871 (m) cm⁻¹. ¹H NMR (400 MHz, CD₂Cl₂): δ 3.26 (s, 4H, CH₂NCH₂), 4.32 (s, CHPh₂), 6.84–7.94 (m, 30H, 6C₆H₅) ppm. ¹³C{¹H} NMR (100 MHz, acetone-*d*₆): δ 53.1–54.8 (m, CH₂NCH₂), 78.8 (s, CHPh₂), 127.7–139.4 (m, C₆H₅) ppm. ³¹P{¹H} NMR (162 MHz, acetone-*d*₆): δ 5.9 (s, PPh₂) ppm.

(iii) [Ph₂CHN(CH₂PPh₂)₂Ni(pdt)Fe(CO)₂(dppe)](BF₄)₂ ([D](BF₄)₂): A 100 mL three-necked flask fitted with a magnetic stir-bar, two serum caps, and a nitrogen inlet tube was charged with [Ph₂CHN(CH₂PPh₂)₂]NiCl₂ (0.355 g, 0.50 mmol), (dppe)Fe(CO)₂(pdt) (0.308, 0.50 mmol), NaBF₄ (0.550 g, 5.0 mmol) and CH₂Cl₂ (30 mL). After the mixture was stirred at 0 °C for 3 h, solvent was removed at reduced pressure and then the residue was subjected to column chromatography (silica gel). Elution with CH₂Cl₂/acetone (*v/v* = 2:1) developed an orange-red band, from which [D](BF₄)₂ (0.571 g, 80%) was obtained as an orange-red solid, mp 170 °C (dec). Anal. calcd for C₇₀H₆₅B₂F₈FeNNiO₂P₄S₂: C, 58.86; H, 4.59; N, 0.98. Found: C, 58.83; H, 4.71; N, 1.13. IR (KBr disk): $\nu_{C\equiv O}$ 1983 (vs) cm⁻¹. ¹H NMR (400 MHz, acetone-*d*₆): δ 2.38–3.99 (m, 14H, CH₂CH₂CH₂, PCH₂CH₂P, CH₂NCH₂), 4.93 (s, 1H, CHPh₂), 6.88–8.00 (m, 50H, 10C₆H₅) ppm. ¹³C{¹H} NMR (100 MHz, acetone-*d*₆): δ 23.3–37.7 (m, CH₂CH₂CH₂, PCH₂CH₂P), 53.0 (s, CH₂NCH₂), 78.1 (CHPh₂), 126.8–139.8 (m, C₆H₅), 209.4, 210.3 (2s, C≡O) ppm. ³¹P{¹H} NMR (162 MHz, acetone-*d*₆): δ 4.9 (s, NiP₂), 56.8 (s, FeP₂) ppm.

[Ph₂CHN(CH₂PPh₂)₂Ni(pdt)Fe(CO)(μ-OH)(dppe)]BF₄ ([6]BF₄): A 50 mL three-necked flask fitted with a magnetic stir-bar, two serum caps, and a nitrogen inlet tube was charged with [D](BF₄)₂ (0.143 g, 0.10 mmol), Me₃NO·2H₂O (0.011 g, 0.10 mmol) and acetone (20 mL) under nitrogen. The mixture was stirred at 0 °C for 4 h. Solvent was removed at reduced pressure and the residue was subjected to column chromatography (silica gel). Elution with CH₂Cl₂/acetone (*v/v* = 10:1) developed an orange-red band, from which [6]BF₄ (0.087 g, 65%) was obtained as an orange-red solid, mp 183–185 °C. Anal. calcd for C₆₉H₆₆BF₄FeNNiO₂P₄S₂: C, 62.28; H, 5.00; N, 1.05. Found: C, 62.11; H, 5.03; N, 1.06. IR (KBr disk): $\nu_{\text{C}\equiv\text{O}}$ 1917 (vs) cm⁻¹. ¹H NMR (400 MHz, acetone-*d*₆): δ -3.39 (s, 1H, OH), 2.20–3.99 (m, 14H, CH₂CH₂CH₂, PCH₂CH₂P, CH₂NCH₂), 4.51 (s, 1H, CHPh₂), 6.66–8.33 (m, 50H, 10C₆H₅) ppm. ¹³C{¹H} NMR (100 MHz, acetone-*d*₆): δ 27.8, 32.3, 37.9 (3s, CH₂CH₂CH₂, PCH₂CH₂P), 55.2 (s, CH₂NCH₂), 78.9 (CHPh₂), 127.9–140.9 (m, C₆H₅), 217.3 (s, C≡O) ppm. ³¹P{¹H} NMR (162 MHz, acetone-*d*₆): δ 2.2 (s, NiP₂), 65.8 (s, FeP₂) ppm.

3.3. Crystal Structure Determinations of Models [A](BF₄)₂, [1]BF₄, [2]BF₄, [4]BF₄, [5]BF₄ and [D](BF₄)₂

While single crystals of [A](BF₄)₂, [1]BF₄, [2]BF₄ and [D](BF₄)₂ for X-ray diffraction analysis were grown by slow diffusion of n-hexane into their CH₂Cl₂ solutions at room temperature, those of [4]BF₄ and [5]BF₄ were grown by slow diffusion of n-hexane into their acetone solutions at room temperature. A single crystal of [A](BF₄)₂, [1]BF₄, [2]BF₄, [4]BF₄ or [5]BF₄ was mounted on a SuperNova, Dual, Cu at zero, AtlasS2 diffractometer, and data were collected using a confocal monochromator with Cu K α radiation (λ = 1.54184 Å) in the ω scanning mode at the temperature of 137 K, 151.6 K, 152 K, 100 K and 293 K, respectively. A single crystal of [D](BF₄)₂ was mounted on a Rigaku Pilatus 200K diffractometer, and data were collected using a confocal monochromator with Mo K α radiation (λ = 0.71073 Å) in the ω scanning mode at the temperature of 113 K. Data collection, reduction, and absorption correction were performed by the CRYSTALCLEAR program [53]. The structures were solved by direct methods using the SHELXT program [54–56] and refined by full-matrix least-squares techniques (SHELXL) [56] on *F*². Hydrogen atoms were located by using the geometric method. Details of the crystal data, data collections, and structure refinements are summarized in Tables S1–S3 of the Supporting Information.

4. Conclusions

Based on the preparation of diphosphine or azadiphosphine-chelated dicarbonyl [NiFe]-H₂ase models [A](BF₄)₂–[D](BF₄)₂, we have further synthesized the corresponding monocarbonyl [NiFe]-H₂ase models [1]BF₄–[6]BF₄ via CO transformation reactions of dicarbonyl complexes [A](BF₄)₂–[D](BF₄)₂. All the new models [A](BF₄)₂, [D](BF₄)₂ and [1]BF₄–[6]BF₄ have been fully characterized by various spectroscopic methods, and particularly for some of them by X-ray crystallography. Of particular interest are (i) dicarbonyl complex [B](BF₄)₂ not only possesses the H₂ activation function to give t-hydride complex [3]BF₄, but also possesses the sp³ C-H bond activation function to afford the novel sp³ C-Fe bond-containing complex [4]BF₄; and (ii) monocarbonyl complexes [2]BF₄ and [5]BF₄ are the first prepared and crystallographically characterized t-isothiocyanato and μ -mercapto ligand-containing [NiFe]-H₂ase models. We believe that the studied results reported here will promote further development of the structural and functional modeling chemistry of [NiFe]-H₂ases.

Supplementary Materials: The following supporting information can be downloaded at: <https://www.mdpi.com/article/10.3390/inorganics10070090/s1>, IR, ¹H NMR, ¹³C{¹H} NMR and ³¹P{¹H} NMR spectra of all the model complexes (Figures S1–S32); crystal data and structure refinement for [A](BF₄)₂, [1]BF₄, [2]BF₄, [4]BF₄, [5]BF₄ and [D](BF₄)₂ (Tables S1–S3).

Author Contributions: L.-C.S. designed and directed the research. S.C., X.-F.H., Z.-Q.Z., Y.-P.W. and Y.-X.D. synthesized and characterized all the new compounds. L.-C.S. acquired funding and wrote the manuscript. All authors have read and agreed to the published version of the manuscript.

Funding: This work was financially supported by the National Natural Science Foundation of China (21772106) and the Ministry of Science and Technology of China (973 program 2014CB845604).

Institutional Review Board Statement: Not applicable.

Informed Consent Statement: Not applicable.

Data Availability Statement: Accession codes CCDC 2173844 for [A](BF₄)₂, CCDC 2173845 for [1]BF₄)₂, CCDC 2173846 for [2]BF₄, CCDC 2173847 for [4]BF₄, CCDC 2173848 for [5]BF₄ and CCDC 2173849 for [D](BF₄)₂ contain the supplementary crystallographic data for this paper. These data can be obtained free of charge from The Cambridge Crystallographic Data Centre via www.ccdc.cam.ac.uk/data_request/cif (accessed on 20 May 2022).

Conflicts of Interest: The authors declare no conflict of interest.

References

1. Adams, M.W.W.; Stiefel, E.I. Biological Hydrogen Production: Not So Elementary. *Science* **1998**, *282*, 1842–1843. [[CrossRef](#)] [[PubMed](#)]
2. Cammack, R. Hydrogenase sophistication. *Nature* **1999**, *397*, 214–215. [[CrossRef](#)] [[PubMed](#)]
3. Schilter, D.; Camara, J.M.; Huynh, M.T.; Hammes-Schiffer, S.; Rauchfuss, T.B. Hydrogenase Enzymes and Their Synthetic Models: The Role of Metal Hydrides. *Chem. Rev.* **2016**, *116*, 8693–8749. [[CrossRef](#)]
4. Albracht, S.P.J. Nickel hydrogenases: In search of the active site. *Biochim. Biophys. Acta* **1994**, *1188*, 167–204. [[CrossRef](#)]
5. Bouwman, E.; Reedijk, J. Structural and functional models related to the nickel hydrogenases. *Coord. Chem. Rev.* **2005**, *249*, 1555–1581. [[CrossRef](#)]
6. Fontecilla-Camps, J.C.; Volbeda, A.; Cavazza, C.; Nicolet, Y. Structure/Function Relationships of [NiFe]- and [FeFe]-Hydrogenases. *Chem. Rev.* **2007**, *107*, 4273–4303. [[CrossRef](#)]
7. Nicolet, Y.; Lemon, B.J.; Fontecilla-Camps, J.C.; Peters, J.W. A novel FeS cluster in Fe-only hydrogenases. *Trends Biochem. Sci.* **2000**, *25*, 138–143. [[CrossRef](#)]
8. Frey, M. Hydrogenases: Hydrogen-Activating Enzymes. *ChemBioChem* **2002**, *3*, 153–160. [[CrossRef](#)]
9. Evans, D.J.; Pickett, C.J. Chemistry and the hydrogenases. *Chem. Soc. Rev.* **2003**, *32*, 268–275. [[CrossRef](#)]
10. Shima, S.; Thauer, R.K. A Third Type of Hydrogenase Catalyzing H₂ Activation. *Chem. Rev.* **2007**, *7*, 37–46. [[CrossRef](#)]
11. Shima, S.; Pilak, O.; Vogt, S.; Schick, M.; Stagni, M.S.; Meyer-Klaucke, W.; Warkentin, E.; Thauer, R.K.; Ermler, U. The Crystal Structure of [Fe]-Hydrogenase Reveals the Geometry of the Active Site. *Science* **2008**, *321*, 572–575. [[CrossRef](#)] [[PubMed](#)]
12. Wright, J.A.; Turrell, P.J.; Pickett, C.J. The Third Hydrogenase: More Natural Organometallics. *Organometallics* **2010**, *29*, 6146–6156. [[CrossRef](#)]
13. Volbeda, A.; Charon, M.-H.; Piras, C.; Hatchikian, E.C.; Frey, M.; Fontecilla-Camps, J.C. Crystal structure of the nickel-iron hydrogenase from *Desulfovibrio gigas*. *Nature* **1995**, *373*, 580–587. [[CrossRef](#)] [[PubMed](#)]
14. Vignais, P.M.; Billond, B.; Meyer, J. Classification and phylogeny of hydrogenases. *FEMS Microbiol. Rev.* **2001**, *25*, 455–501. [[CrossRef](#)]
15. Volbeda, A.; Garcin, E.; Piras, C.; De Lacey, A.L.; Fernandez, V.M.; Hatchikian, E.C.; Frey, M.; Fontecilla-Camps, J.C. Structure of the [NiFe] Hydrogenase Active Site: Evidence for Biologically Uncommon Fe Ligands. *J. Am. Chem. Soc.* **1996**, *118*, 12989–12996. [[CrossRef](#)]
16. Higuchi, Y.; Ogata, H.; Miki, K.; Yasuoka, N.; Yagi, T. Removal of the bridging ligand atom at the Ni–Fe active site of [NiFe] hydrogenase upon reduction with H₂, as revealed by X-ray structure analysis at 1.4 Å resolution. *Structure* **1999**, *7*, 549–556. [[CrossRef](#)]
17. Matias, P.M.; Soares, C.M.; Saraiva, L.M.; Coelho, R.; Morais, J.; Le Gall, J.; Carrondo, M.A. [NiFe] hydrogenase from *Desulfovibrio desulfuricans* ATCC 27774: Gene sequencing, three-dimensional structure determination and refinement at 1.8 Å and modelling studies of its interaction with the tetrahaem cytochrome c₃. *J. Biol. Inorg. Chem.* **2001**, *6*, 63–81. [[CrossRef](#)]
18. Volbeda, A.; Martin, L.; Cavazza, C.; Matho, M.; Faber, B.W.; Roseboom, W.; Albracht, S.P.J.; Garcin, E.; Rousset, M.; Fontecilla-Camps, J.C. Structural differences between the ready and unready oxidized states of [NiFe] hydrogenases. *J. Biol. Inorg. Chem.* **2005**, *10*, 239–249. [[CrossRef](#)]
19. Ogata, H.; Nishikawa, K.; Lubitz, W. Hydrogens detected by subatomic resolution protein crystallography in a [NiFe] hydrogenase. *Nature* **2015**, *520*, 571–574. [[CrossRef](#)]
20. Wang, H.; Yoda, Y.; Ogata, H.; Tanaka, Y.; Lubitz, W. A strenuous experimental journey searching for spectroscopic evidence of a bridging nickel–iron–hydride in [NiFe] hydrogenase. *J. Synchrotron Rad.* **2015**, *22*, 1334–1344. [[CrossRef](#)]
21. Ogo, S. H₂ and O₂ activation by [NiFe]hydrogenases—Insights from model complexes. *Coord. Chem. Rev.* **2017**, *334*, 43–53. [[CrossRef](#)]
22. Bose, M.; Li, Z.; Matsumoto, T.; Tatsumi, K. A Dithiolato and Hydrido Bridged (CO/CN)Fe–Ni Complex with Unprotected CN: A Model for the [Ni–R] State of the [Ni–Fe] Hydrogenase Active Site. *Inorg. Chem.* **2020**, *59*, 968–971. [[CrossRef](#)] [[PubMed](#)]

23. Lindenmaier, N.J.; Wahlefeld, S.; Bill, E.; Szilvási, T.; Eberle, C.; Yao, S.; Hildebrandt, P.; Horch, M.; Zebger, I.; Driess, M. An S-Oxygenated [NiFe] Complex Modelling Sulfenate Intermediates of an O₂-Tolerant Hydrogenase. *Angew. Chem. Int. Ed.* **2017**, *56*, 2208–2211. [[CrossRef](#)] [[PubMed](#)]
24. Perotto, C.U.; Sodipo, C.L.; Jones, G.J.; Tidey, J.P.; Blake, A.J.; Lewis, W.; Davies, E.S.; McMaster, J.; Schröder, M. Heterobimetallic [NiFe] Complexes Containing Mixed CO/CN⁻ Ligands: Analogs of the Active Site of the [NiFe] Hydrogenases. *Inorg. Chem.* **2018**, *57*, 2558–2569. [[CrossRef](#)]
25. Osterloh, F.; Saak, W.; Haase, D.; Pohl, S. Synthesis, X-ray structure and electrochemical characterisation of a binuclear thiolate bridged Ni-Fe-nitrosyl complex, related to the active site of NiFe hydrogenase. *Chem. Commun.* **1997**, 979–980. [[CrossRef](#)]
26. Song, L.-C.; Lu, Y.; Zhu, L.; Li, Q.-L. Dithiolato- and Diselenolato-Bridged Nickel-Iron Biomimetics for the Active Site of [NiFe]Hydrogenases. *Organometallics* **2017**, *36*, 750–760. [[CrossRef](#)]
27. Jiang, J.; Maruani, M.; Solaimanzadeh, J.; Lo, W.; Koch, S.A.; Millar, M. Synthesis and Structure of Analogues for the Ni-Fe Site in Hydrogenase Enzymes. *Inorg. Chem.* **2009**, *48*, 6359–6361. [[CrossRef](#)] [[PubMed](#)]
28. Sellmann, D.; Geipel, F.; Lauderbach, F.; Heinemann, F.W. [(C₆H₄S₂)Ni(μ-S₃)Fe(CO)(PMe₃)₂]: A Dinuclear [NiFe] Complex Modeling the [(RS)₂Ni(μ-SR)₂Fe(CO)(L)₂] Core of [NiFe] Hydrogenase Centers. *Angew. Chem. Int. Ed.* **2002**, *41*, 632–634. [[CrossRef](#)]
29. Smith, M.C.; Barclay, J.E.; Cramer, S.P.; Davies, S.C.; Gu, W.-W.; Hughes, D.L.; Longhurst, S.; Evans, D.J. Nickel-iron-sulfur complexes: Approaching structural analogues of the active sites of NiFe-hydrogenase and carbon monoxide dehydrogenase/acetyl-CoA synthase. *J. Chem. Soc., Dalton Trans.* **2002**, *13*, 2641–2647. [[CrossRef](#)]
30. Verhagen, J.A.W.; Lutz, M.; Spek, A.L.; Bouwman, E. Synthesis and Characterisation of New Nickel-Iron Complexes with an S₄ Coordination Environment around the Nickel Centre. *Eur. J. Inorg. Chem.* **2003**, *2003*, 3968–3974. [[CrossRef](#)]
31. Li, Z.; Ohki, Y.; Tatsumi, K. Dithiolato-Bridged Dinuclear Iron-Nickel Complexes [Fe(CO)₂(CN)₂(μ-SCH₂CH₂CH₂S)Ni(S₂CNR₂)] Modeling the Active Site of [NiFe] Hydrogenase. *J. Am. Chem. Soc.* **2005**, *127*, 8950–8951. [[CrossRef](#)] [[PubMed](#)]
32. Sellmann, D.; Lauderbach, F.; Heinemann, F.W. Trinuclear [NiFe] Clusters as Structural Models for [NiFe] Hydrogenase Active Sites. *Eur. J. Inorg. Chem.* **2005**, *2005*, 371–377. [[CrossRef](#)]
33. Ogo, S.; Ichikawa, K.; Kishima, T.; Matsumoto, T.; Nakai, H.; Kusaka, K.; Ohhara, T. A Functional [NiFe]Hydrogenase Mimic That Catalyzes Electron and Hydride Transfer from H₂. *Science* **2013**, *339*, 682–684. [[CrossRef](#)] [[PubMed](#)]
34. Ohki, Y.; Yasumura, K.; Ando, M.; Shimokata, S.; Tatsumi, K. A model for the CO-inhibited form of [NiFe] hydrogenase: Synthesis of (CO)₃Fe(μ-S^tBu)₃Ni{SC₆H₃-2,6-(mesityl)₂} and reversible CO addition at the Ni site. *Proc. Natl. Acad. Sci. USA* **2010**, *107*, 3994–3997. [[CrossRef](#)]
35. Song, L.-C.; Li, J.-P.; Xie, Z.-J.; Song, H.-B. Synthesis, Structural Characterization, and Electrochemical Properties of Dinuclear Ni/Mn Model Complexes for the Active Site of [NiFe]-Hydrogenases. *Inorg. Chem.* **2013**, *52*, 11618–11626. [[CrossRef](#)]
36. Brazzolotto, D.; Wang, L.; Tang, H.; Gennari, M.; Queyriaux, N.; Philouze, C.; Demeshko, S.; Meyer, F.; Orio, M.; Artero, V.; et al. Tuning Reactivity of Bio-inspired [NiFe]-Hydrogenase Models by Ligand Design and Modeling the CO Inhibition Process. *ACS Catal.* **2018**, *8*, 10658–10667. [[CrossRef](#)]
37. Song, L.-C.; Chen, W.; Feng, L. Two heterodinuclear NiFe-based sulfenate complexes mimicking an S-oxygenated intermediate of an O₂-tolerant [NiFe]-H₂ase: Synthesis, structures, and reactivity. *New J. Chem.* **2020**, *44*, 14015–14023. [[CrossRef](#)]
38. Song, L.-C.; Feng, L.; Lu, Y.; Yang, X.-Y. Synthesis, Structures and Reactivity of [NiFe]-H₂ase Mimics Containing One Square-Planar N₂S₂ Ligand Bridged between Their Ni/Fe Centers through One or Two S Atoms. *Organometallics* **2021**, *40*, 508–519. [[CrossRef](#)]
39. Lubitz, W.; Tumas, W. Hydrogen: An Overview. *Chem. Rev.* **2007**, *107*, 3900–3903. [[CrossRef](#)]
40. Simmons, T.R.; Berggren, G.; Bacchi, M.; Fontcave, M.; Artero, V. Mimicking hydrogenases: From biomimetics to artificial enzymes. *Coord. Chem. Rev.* **2014**, *270–271*, 127–150. [[CrossRef](#)]
41. Ogo, S.; Kishima, T.; Yatabe, T.; Miyazawa, K.; Yamasaki, R.; Matsumoto, T.; Ando, T.; Kikkawa, M.; Isegawa, M.; Yoon, K.-S.; et al. [NiFe], [FeFe], and [Fe]hydrogenase models from isomers. *Sci. Adv.* **2020**, *6*, eaaz8181. [[CrossRef](#)] [[PubMed](#)]
42. Song, L.-C.; Yang, X.-Y.; Cao, M.; Gao, X.-Y.; Liu, B.-B.; Zhu, L.; Jiang, F. Dithiolato-Bridged Nickel-Iron Complexes as Models for the Active Site of [NiFe]-Hydrogenases. *Chem. Commun.* **2017**, *53*, 3818–3821. [[CrossRef](#)] [[PubMed](#)]
43. Song, L.-C.; Yang, X.-Y.; Gao, X.-Y.; Cao, M. Nickel-Iron Dithiolato Hydrides Derived from H₂ Activation by Their μ-Hydroxo Ligand-Containing Analogues. *Inorg. Chem.* **2019**, *58*, 39–42. [[CrossRef](#)] [[PubMed](#)]
44. Song, L.-C.; Liu, B.-B.; Liu, W.-B.; Tan, Z.-L. Heterodinuclear nickel(II)-iron(II) azadithiolates as structural and functional models for the active site of [NiFe]-hydrogenases. *RSC Adv.* **2020**, *10*, 32069–32077. [[CrossRef](#)] [[PubMed](#)]
45. Song, L.-C.; Gao, X.-Y.; Liu, W.-B.; Zhang, H.-T.; Cao, M. Synthesis, Characterization, and Reactions of Functionalized Nickel-Iron Dithiolates Related to the Active Site of [NiFe]-Hydrogenases. *Organometallics* **2018**, *37*, 1050–1061. [[CrossRef](#)]
46. Cordero, B.; Gómez, V.; Platero-Prats, A.E.; Revés, M.; Echeverría, J.; Cremades, E. Barragán, F.; Alvarez, S. Covalent radii revisited. *Dalton Trans.* **2008**, *21*, 2832–2838. [[CrossRef](#)]
47. Manor, B.C.; Rauchfuss, T.B. Hydrogen Activation by Biomimetic [NiFe]-Hydrogenase Model Containing Protected Cyanide Cofactors. *J. Am. Chem. Soc.* **2013**, *135*, 11895–11900. [[CrossRef](#)]
48. Collman, J.P.; Hegedus, L.S. *Principles and Applications of Organotransition Metal Chemistry*; University Science Books: Mill Valley, CA, USA, 1980.

49. Tanino, S.; Li, Z.; Ohki, Y.; Tatsumi, K. A dithiolate-bridged (CN)₂(CO)Fe-Ni complex reproducing the IR bands of [NiFe] hydrogenase. *Inorg. Chem.* **2009**, *48*, 2358–2360. [[CrossRef](#)]
50. Shang, R.; Ilies, L.; Nakamura, E. Iron-Catalyzed C–H Bond Activation. *Chem. Rev.* **2017**, *117*, 9086–9139. [[CrossRef](#)]
51. Gray, L.R.; Higgins, S.J.; Levason, W.; Webster, M. Co-ordination chemistry of higher oxidation states. Part 8. Nickel(III) complexes of bi- and multi-dentate phosphorus and arsenic ligands; crystal and molecular structure of [Ni(Ph₂PCH₂CH₂PPh₂)Br₃]-C₆H₅Me. *J. Chem. Soc. Dalton Trans.* **1984**, 459–467. [[CrossRef](#)]
52. Carroll, M.E.; Chen, J.; Gray, D.E.; Lansing, J.C.; Rauchfuss, T.B.; Schilter, D.; Volkers, P.I.; Wilson, S.R. Ferrous Carbonyl Dithiolates as Precursors to FeFe, FeCo, and FeMn Carbonyl Dithiolates. *Organometallics* **2014**, *33*, 858–867. [[CrossRef](#)] [[PubMed](#)]
53. *CrystalClear and CrystalStructure*; Rigaku and Rigaku Americas: The Woodlands, TX, USA, 2007.
54. Sheldrick, G.M. *SHELXS-97 and SHELXL-97, Program for Crystal Structure Solution and Refinement*; University of Göttingen: Göttingen, Germany, 1997.
55. Sheldrick, G.M. A short history of SHELX. *Acta Crystallogr. Sect. A Found. Crystallogr.* **2008**, *64*, 112–122. [[CrossRef](#)] [[PubMed](#)]
56. Sheldrick, G.M. SHELXT-Integrated space-group and crystal-structure determination. *Acta Crystallogr. Sect. A Found. Adv.* **2015**, *71*, 3–8. [[CrossRef](#)] [[PubMed](#)]